Internal wave generation from rough topography

D. A. Aguilar and B. R. Sutherland[a)]
Department of Mathematical and Statistical Sciences, University of Alberta, Edmonton, Alberta T6G 2G1, Canada

(Received 9 January 2006; accepted 21 May 2006; published online 30 June 2006)

Through laboratory experiments we examine internal wave generation above and in the lee of finite-amplitude periodic topography having various degrees of roughness. We show that internal waves are generated not only by flow over the hills but also by flow over "boundary-trapped" lee waves and by vigorous turbulence created in the lee of sharp-crested hills. For low values of the excitation frequency, linear theory well predicts the internal wave frequencies but significantly overestimates the wave amplitudes because it neglects processes associated with boundary layer separation. When the excitation frequency exceeds the buoyancy frequency, turbulence results in the excitation of internal waves with frequencies approximately 0.72 ± 0.05 of the buoyancy frequency and vertical displacement amplitudes ranging between 1.5% and 2% of the horizontal wavelength. © *2006 American Institute of Physics*. [DOI: 10.1063/1.2214538]

I. INTRODUCTION

In general, internal waves are generated whenever a stratified fluid is perturbed at a frequency smaller than the buoyancy frequency, which is the natural frequency of vertical oscillation of the fluid. The waves subsequently propagate horizontally and vertically within the fluid, transporting energy and momentum away from their source.

A significant source of internal waves in the atmosphere and ocean is through the flow of stratified fluid over mountains or submarine ridges. In the atmosphere, such topographically generated waves significantly influence the general circulation of the atmosphere.[1,2] In the abyssal ocean, slow frequency internal waves are generated largely due to tidal flow over topography, their characteristics determined by the slope of the topography relative to the slope of the internal wavebeams.[3–8] On time scales that are short compared to the tidal period, one can assume internal waves are generated by an approximately steady, unidirectional flow as is the case in the atmosphere. However, observations reveal that energetic turbulence and associated internal wave activity is most significant over the rough terrain of the ocean floor, such as near sea mounts, ridges, and canyons.[9,10,6,11–13] This raises the question: What is the importance of such rough features upon wave excitation?

Analytic theories for topographically generated waves include linear theory,[14] which assumes the hill height is small, and Long's theory,[15] which considers steady flow over finite-amplitude hills. Both theories are limited in that they assume that the topographic surface is a streamline. However, if the topography is rough or if the hills are sufficiently steep, we expect the flow will separate from the boundary leading both to regions of blocked fluid beneath the separation point and to downstream turbulence. Such effects upon the generation of internal waves are poorly understood and form the focus of the experimental study reported upon here.

The characteristics of internal waves generated by the steady flow of uniformly stratified fluid over topography depend upon the flow speed, U, the characteristic horizontal (L), and vertical (H) scales of the hills, and the buoyancy frequency, N, given in the Boussinesq approximation by

$$N^2 = -\frac{g}{\rho_0}\frac{d\bar{\rho}}{dz}, \tag{1}$$

in which $\bar{\rho}(z)$ is the background density, ρ_0 the characteristic density, and g is the acceleration due to gravity.

If the topography is small amplitude and sinusoidal with wave number k and crest-to-crest distance $L \equiv 2\pi/k$, then uniform flow will perturb the fluid at an excitation frequency

$$\omega_{\text{exc}} \equiv Uk. \tag{2}$$

Defining the Froude number by

$$\text{Fr} \equiv \frac{\omega_{\text{exc}}}{N} = \frac{Uk}{N}, \tag{3}$$

linear theory predicts that the disturbances are evanescent if $\text{Fr} > 1$ and that vertically propagating internal waves are generated if $\text{Fr} < 1$. By analogy with shallow water theory, the flow is said to be subcritical or supercritical depending on whether $\text{Fr} < 1$ or $\text{Fr} > 1$, respectively.[16]

A measure of the importance of nonlinearity upon stratified flow is sometimes represented by the nondimensional quantity NH/U or its inverse. There is no standard symbol for this quantity in the literature,[16] so for convenience here we will call it Long's number, after the pioneering experimentalist and theorist who studied stratified flow over topography.[15,17,18] Thus, we define

$$\text{Lo} \equiv \frac{NH}{U}. \tag{4}$$

Sometimes the linear theory regime is assumed to be represented by the limit $\text{Lo} \ll 1$, but this can be misleading. If the fluid in unstratified, the hills can be arbitrarily large am-

[a)]Author to whom correspondence should be addressed.

plitude although Lo=0. Even weakly stratified flow over small amplitude hills is turbulent for sufficiently large U.

A better interpretation is that the magnitude of Lo represents the importance of stratification upon boundary layer separation. For fixed H and U, the flow will separate for sufficiently large N, and hence large Lo, simply because the flow does not possess enough kinetic energy to rise over a hill or to sweep dense fluid out of a valley. For small Lo, boundary layer separation may still occur but due to adverse pressure gradients in the lee of a hill crest that develop through dynamics independent of stratification. For large Reynolds number flow, in this case the shape of the hills, not just their height, plays the most important role in determining whether or not separation occurs.

The effect of Lo upon boundary layer separation in two-dimensional geometries has been examined experimentally for flow over valleys[16] and in the lee of isolated hills.[19] The latter showed that for a limited range of Lo, flow separation resulted in the development of an undular disturbance, a "boundary-trapped lee wave," initiated by low pressure and restoring buoyancy forces that displaced fluid downward in the lee of the hills. In the lee of a smooth step, the lee waves always occurred being initiated by low pressure alone. These had frequency moderately smaller than the background buoyancy frequency.[20]

The first study of the impact of boundary layer separation upon internal wave generation used numerical simulations to examine the formation of blocked layers between finite-amplitude sinusoidal hills.[21] Blocked layers formed when Lo exceeded a threshold between 0.5 and 1. Above this threshold, the blocked-layer height increased linearly with H so that, with respect to the waves, the effective hill height, H_{eff}, was relatively constant. This suggested that topographically generated internal waves have limited amplitude.

These results were consistent with the experimental-theoretical study of Aguilar *et al.*,[22] who examined internal waves generated (effectively) above and in the lee of a train of sinusoidal hills having moderate and large amplitude. As well as examining the wave amplitude above the hills for $\text{Fr}<1$, the experiments showed that waves with nearly constant frequency, $0.5N$, were generated in the lee of the hills for a wide range of supercritical Froude numbers.

The experiments further suggested that decaying turbulence also generates internal waves in the far lee, typically beyond a distance U/N. Beyond idealized theory,[23] and a few laboratory experiments,[24–27] relatively little is known about turbulence as a generation mechanism of internal waves. In part, the experiments presented here aim to provide further insight into these dynamics.

Specifically, we examine stratified flow over finite-amplitude periodic topography with sinusoidal, triangular and rectangular shapes. The experiments are designed to examine the effect of sharp boundaries upon boundary layer separation and consequent wave generation above and in the near and far lee of the hills.

In Sec. II we introduce the experimental setup, including methods for wave visualization and techniques for determining wave properties such as frequency, wave number, and amplitude. In Sec. III we present the experimental results for flow over and in the near lee of sinusoidal, triangular and rectangular hills. The flow over steep hills also results in significant turbulent mixing far in their lee. In these circumstances we also examine wave generation by downstream turbulence. We summarize our significant findings in Sec. IV.

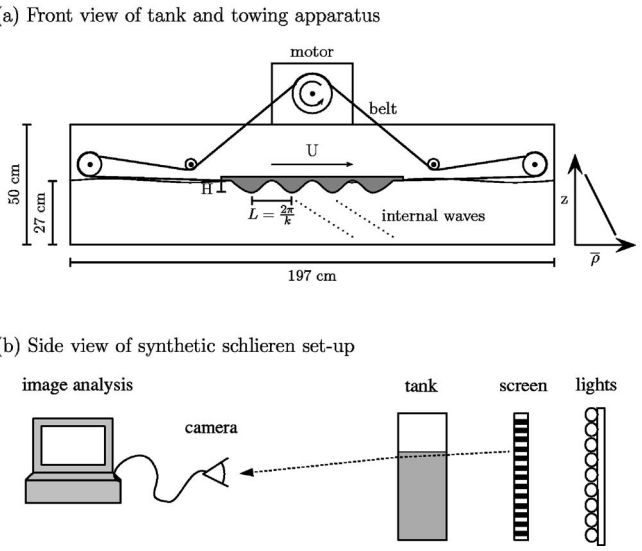

FIG. 1. (a) Front view of tank and towing apparatus. The motor is mounted above the tank. A belt is attached to the topography and runs around a series of pulleys. When the motor is turned on, the topography moves from left to right at an approximately constant speed, thus exciting internal waves. (b) Side view of the experimental configuration for the synthetic Schlieren technique. The technique records the distortion of the image of horizontal lines due to density fluctuations within the tank. The density fluctuations are the result of internal wave motion.

II. EXPERIMENTAL SETUP AND ANALYSIS

A. Apparatus

Experiments were performed in a glass tank having dimensions 197 cm long by 50 cm high by 17.5 cm wide. The tank was filled with uniformly salt-stratified water to a depth of approximately 27 cm. This was accomplished using the standard "double-bucket" technique.[28] The resulting background density field, $\bar{\rho}(z)$, was measured by traversing a conductivity probe down through the tank before each experiment. A schematic illustrating the tank dimensions and a typical background density profile is given in Fig. 1(a). The buoyancy frequency was determined directly from the slope of the best-fit line to the density profile. Typically, its value was $N=1.10\pm0.02\ \text{s}^{-1}$, although some experiments were performed with N as large as $2.26\ \text{s}^{-1}$.

We used four model hills each spanning the tank width but having different along-tank shapes: two sinusoidal hills had peak-to-peak heights $H=0.65$ cm and 1.30 cm, and the triangular and rectangular hills both had height $H=1.30$ cm. For all four sets of hills, the crest-to-crest distance was $L=13.7$ cm and each set included four wavelengths, as sketched in Fig. 1.

To simulate uniform flow over topography, model hills were towed along the surface of the fluid at an approximately constant speed, U. This was achieved using a towing apparatus consisting of a motor, five pulleys, and a belt that was

fixed to the model topography. The model hills were towed at speeds ranging from $U=0.8$ to 5.2 cm/s. The corresponding Froude and Long numbers ranged between Fr $\sim 0.2-2.1$ and Lo $\sim 0.29-6.07$.

The Reynolds number, based on L, ranged from Re ~ 1000 to 5000. Although significantly smaller than typical ocean and atmospheric values, the experimental values were still large enough that viscous effects would be important only insofar as boundary layer separation and turbulence damping time scales are concerned.

Although the fluid had finite depth, the experiments were performed over such short durations ($\approx 30-80$ s) that vertically propagating internal waves did not reach the tank bottom before the experiment finished. Thus, the effect of the bottom boundary was essentially negligible and the experiments effectively modelled wave propagation in an infinite-depth fluid.

Before the start of each experiment, potassium permanganate crystals were laid down in front of the hills, forming a straight vertical dye-line. The movement of the model hills through the fluid produced a reverse background flow, which caused a net deceleration of the near-hill fluid. This background flow was clearly visualized by the movement of the dye-line from its original position. To determine whether or not the average background flow speed, U_b, was significant compared to the towing speed, it was approximated for eight experiments, covering a range of Fr and Lo. This was done by measuring the average displacement of the dye-line over three hill periods. In most cases, the background flow speed was only 5%–20% of the towing speed, not high enough to have a significant effect on the results. However, for Lo $\gtrsim 3$, we found $U_b \gtrsim 0.3U$. In these extreme circumstances, the influence of the undercurrent should be taken into account when interpreting the results.

B. Synthetic Schlieren analyses

The experiments were recorded using a digital camera situated approximately 340 cm in front of the tank. Recorded images in the x-z plane were analyzed using the image processing software package, DigImage.[29]

Synthetic Schlieren, the configuration of which is illustrated schematically in Fig. 1(b), nonintrusively measured the two-dimensional internal wave field as it evolved in time.[30] The technique exploits how light is deflected to a greater or lesser degree as it passes respectively through stronger or weaker density gradients. With straightforward computer processing,[31] distortions of an image of horizontal black and white lines were used to measure vertical derivatives of perturbation density which, for convenience, were recast in terms of the ΔN^2. This is the change in the background density gradient due to the stretch and compression of isopycnals by internal waves. Likewise, we can determine changes to ΔN^2 between small times ($\Delta t \sim 1/15-3/15$ s) and so compute the time derivative N_t^2.

For the purposes of performing qualitative and quantitative analyses, the N_t^2 field was preferred for three reasons: it was in phase with the vertical displacement field, ξ; it could be determined even for moderate-amplitude waves, which significantly distorted the background image, and it filtered long time scale variations thus capturing the signal from relatively short time scale propagating waves alone.

The half peak-to-peak amplitude of the N_t^2 field, $A_{N_t^2}$, was determined by taking the root-mean-squared average in time and then multiplying by a factor of $2^{1/2}$. The result was spatially averaged within a window selected to isolate the waves of interest. Generally the window extended across a minimum of one horizontal and vertical wavelength beginning at least 5 cm above the hill crests. This lower bound was sufficiently far from the local mixing region where the Schlieren technique did not accurately measure N_t^2.

Vertical wave numbers, k_z, and frequencies, ω, were determined from power spectra of vertical time series of N_t^2, and horizontal wave numbers, k_x, and frequencies were likewise determined from horizontal time series.[22] Which type of time series used depended upon the horizontal and vertical scale of the waves.

Vertically propagating waves had phase lines tilted at an angle Θ to the vertical, which was estimated from the relative wave frequency using the dispersion relation

$$\omega = N \cos\Theta = \frac{|k_x|}{\sqrt{k_x^2 + k_z^2}}. \tag{5}$$

The vertical displacement amplitude, A_ξ, was estimated from $A_{N_t^2}$ using the polarization relations for Boussinesq small-amplitude plane waves in a uniformly stratified fluid:

$$A_{N_t^2} = 2\pi N^3 \sin\Theta \frac{A_\xi}{\lambda_x}. \tag{6}$$

C. Wave-induced drag

Linear theory predicts that small amplitude sinusoidal hills with wave number k and half peak-to-peak amplitude A_ξ excite waves with the same horizontal wave number and amplitude. The drag on the hills due to wave generation is given by the period-averaged vertical flux of horizontal momentum, $F_{D,thy}$, associated with the waves. Explicitly,

$$F_{D,thy} = \frac{1}{4}\rho_0 N^2 \sin(2\Theta) A_\xi^2, \tag{7}$$

in which Θ is given by (5).

If the hills are such large amplitude or so sharp that boundary layers separate from the hills and fluid is trapped in the valleys between hills, then the amplitude of the waves is smaller than the hill amplitude. From numerical simulations, Welch *et al.*[21] developed an empirical theory for the actual drag, F_D, as a function of Lo:

$$\frac{F_D}{F_{D,thy}} \approx \frac{\mathcal{H}}{\pi}\{\cos^{-1}[1-2\mathcal{H}] - 2[1-2\mathcal{H}]\sqrt{\mathcal{H}(1-\mathcal{H})}\}. \tag{8}$$

Here

$$\mathcal{H} = \begin{cases} 1 & \text{Lo} \leqslant \text{Lo}_c \\ \text{Lo}_c/\text{Lo} & \text{Lo} > \text{Lo}_c \end{cases} \tag{9}$$

and Lo_c is the critical value of Lo above which the effects of boundary layer separation and blocking act to reduce the

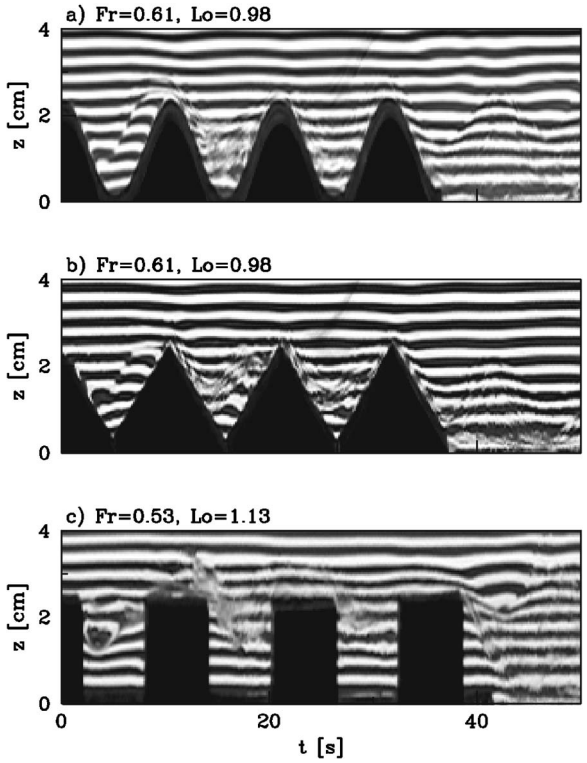

FIG. 2. Sample vertical time series of the near-hill region for subcritical flow, illustrating the flow pattern above and in the near-lee of (a) sinusoidal, (b) triangular, and (c) rectangular hills.

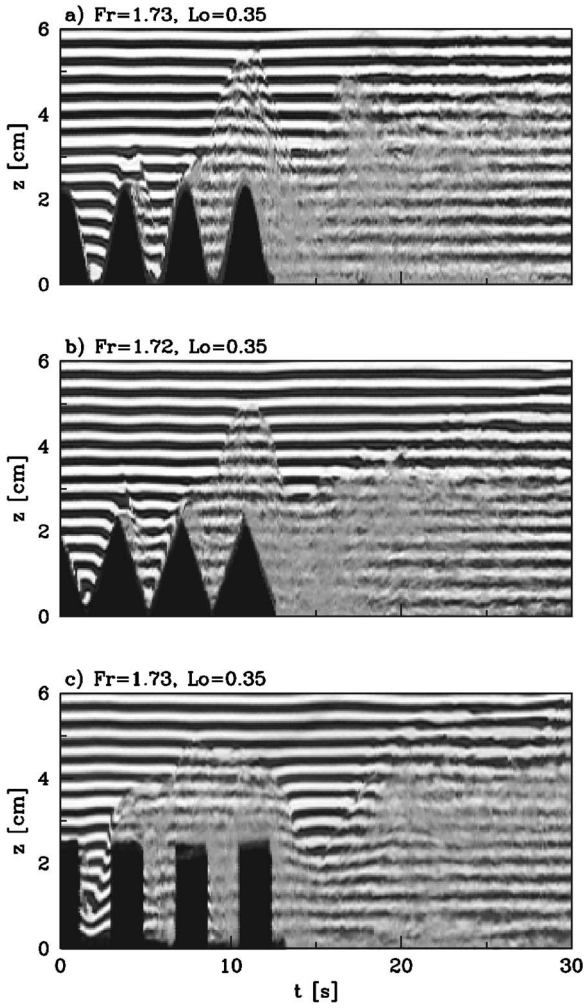

FIG. 3. As in Fig. 2 but showing vertical time series taken from three experiments with supercritical flow.

wave-induced drag from the value predicted by linear theory. In our experiments we expect the critical value to be lowest for waves generated over the rectangular hills.

III. RESULTS

A. Qualitative observations

We first discuss the qualitative structure of the flow in the near hill region. This is done by examining vertical time series images showing how the image of horizontal black-and-white lines behind the tank is distorted by perturbed density gradients within the tank itself. The pattern of distortions reveals where boundary layer separation occurs and indicates the presence of turbulence where the image blurs. For conceptual convenience the images have been flipped vertically. In the Boussinesq approximation, appropriate for salt-stratified fluids, there is no dynamical difference between disturbances generated below topography towed along the top of the tank and disturbances generated above the bottom topography.

Figure 2 shows images of the near-hill region for comparable subcritical Froude number experiments run with large-amplitude sinusoidal, triangular, and rectangular topography. Each time series is constructed from a vertical slice taken through movies of the experiment at the midpoint of the crest of the leading hill. The hills begin to move at time $t=0$ and the resulting flow is shown as the trailing three hills move past that position.

As is typical for a number of experiments, the flow structure behind the leading crest is similar for the sinusoidal and triangular hills. The separation point occurs at the same distance, about $3/4H$ below the leading crest and the separated streamline rises to meet the following crest. In both experiments, a undulating "boundary-trapped lee wave" is evident behind the last hill, peaking in both cases around time $t=42$ s.

In contrast, the image is more greatly distorted in the lee of the leading rectangular hill crest [Fig 2(c)], indicating a more complicated flow pattern associated with boundary layer separation. Indeed, movies of this experiment clearly reveal the detachment of the streamline from the corner of the hills and the ensuing development of a Kelvin-Helmholtz billows in their lee. Although the separated flow dips downward slightly behind the lee of the trailing hill, the downstream flow exhibits a more turbulent, less coherent undular wake. For fixed Fr, generally we find that more fluid is trapped in the valleys between the rectangular hills than between sinusoidal or triangular hills.

Figure 3 shows three corresponding time series images for experiments having supercritical Froude numbers Fr $\simeq 1.7$ and Lo $\simeq 0.35$. Again, the flow is similar for the sinusoidal and triangular hills. The image distorts little in the valley behind the leading crest but the disturbance resulting

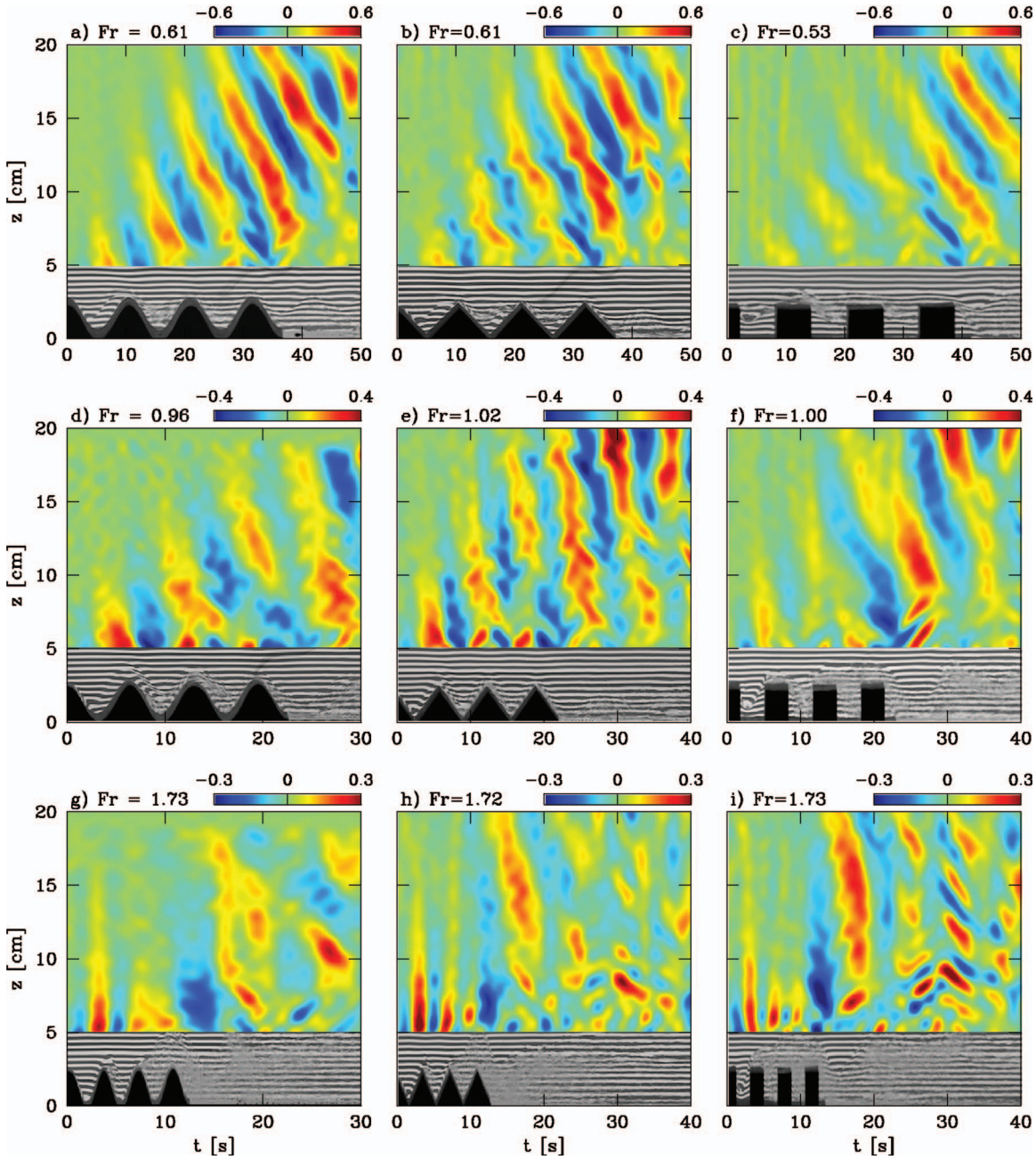

FIG. 4. (Color) Vertical time series of N_t^2 (s^{-3}) for the sinusoidal, triangular and rectangular hills for the cases of (a, b, c) $Fr<1$, (d, e, f) $Fr\gtrsim 1$, and (g, h, i) $Fr>1$. Vertical time series of the near-hill region of the raw images are superimposed to help visualize the vertically propagating internal waves relative to the topography and boundary-trapped lee waves. [Movies corresponding to Figs. 4(a)–4(c) and 4(i) are available online.]

from boundary layer separation grows a full hill height above the last hill. Conversely, the image is greatly distorted behind and above all three trailing rectangular hills.

All three experiments exhibit a descending streamline separating laminar and turbulent flow in the near lee of trailing hill. Further downstream the turbulent flow grows as deep as three hill heights. A range of experiments show this growth is most substantial in the lee of the rectangular hills and least substantial behind the triangular hills.

Next we qualitatively examine the resulting structure of internal waves generated above and in the lee of the hills. Figure 4 shows nine composite vertical time series in which the raw gray scale image is shown up to 5 cm above the base of the hills and the computed N_t^2 field is shown by color contours between 5 and 20 cm. We do not show the N_t^2 field below 5 cm because its computation is inaccurate where the image is highly distorted.

Figures 4(a)–4(c) show the three subcritical cases corresponding to the images in Figs. 2 (enhanced with video online). In all three, waves are generated over the hills with comparable horizontal wavelengths and retrograde-tilting phase lines. For the rectangular hills, the wave amplitude is significantly lower directly over the hills, a result of more fluid being trapped between the hills.

The waves grow in amplitude in the near-lee of the hills in these three subcritical flow experiments as a result of the

flow that descends, uninhibited by valley-trapped fluid behind the trailing hill. Despite the change in forcing conditions, the horizontal wavelength and tilt of phase lines in the lee are comparable to those over the hills. Furthermore, we find that the horizontal distance between trough and crest of the propagating lee waves is comparable to the corresponding distance for the underlying boundary-trapped lee wave.

Three near-critical flow cases are illustrated in Figs. 4(d)–4(f). Although linear theory predicts that phase lines should be nearly vertical in this circumstance, we nonetheless observe retrograde tilting phase lines corresponding to vertically propagating waves. These are most clearly evident above sinusoidal and triangular topography.

Vertically propagating lee waves are evident in all three cases. However, unlike the subcritical cases examined above, here we see that the amplitude is largest in the lee of rectangular topography.

Still further in the lee, the boundary-trapped lee wave breaks up into a patch of turbulence, above which some smaller-scale wave structures begin to emerge ($t \approx 40$ s). These smaller-scale waves also appear for the triangular hills but only for $\mathrm{Fr} > 1$. This is because flow over the triangular hills does not create as much turbulence as that over the rectangular hills for a given flow speed, U.

Figures 4(g)–4(i) present three supercritical cases corresponding to the near-hill images shown in Fig. 3. [Fig. 4(i) enhanced with video online.] In all three cases the disturbances are evanescent directly over the hills: the phase lines are vertical and decrease in amplitude with height. As in the three critical cases, boundary-trapped lee waves and corresponding vertically propagating lee waves are clearly visible and the wave amplitudes are slightly larger for the rectangular hills. Further downstream, and particularly in the lee of rectangular topography, we observe relatively small vertical scale internal waves radiating away from the decaying turbulent mixed region around time $t \sim 30$ s. The structure of the waves is remarkably coherent given the random nature of their turbulent source.

B. Quantitative results

From the spectra of the vertical time series taken during the passage of the hills, immediately in their lee (within two buoyancy periods of the passage of the last hill) and in their far lee (beyond two buoyancy periods), we determine the relative frequency of internal waves generated, respectively, by the hills, by the flow in the lee, and by the decaying turbulence far downstream. The results are plotted in Fig. 5. For reference, on all three we plot the line corresponding to $\omega = N\mathrm{Fr} = \omega_{\mathrm{exc}}$, which is the wave frequency predicted by linear theory to occur due to flow over small amplitude sinusoidal hills.

For all three topographic shapes, the waves generated directly over the hills have frequencies that agree well with linear theory predictions for $\mathrm{Fr} < 0.7$. In particular, we find that the pronounced effect of boundary layer separation above rectangular hills does not significantly influence the resulting wave frequencies. For $0.7 < \mathrm{Fr} < 1$, the observed

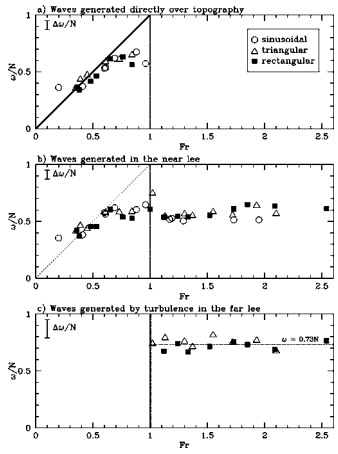

FIG. 5. Plot of measured relative internal wave frequency, ω/N, as a function of $\mathrm{Fr} = \omega_{\mathrm{exc}}/N$ for (a) waves generated directly over, (b) in the lee and (c) in the far lee of large-amplitude sinusoidal, triangular and rectangular hills, as indicated in the legend. The solid line in (a) and the short-dashed line in (b) corresponds to $\omega = \omega_{\mathrm{exc}}$, which is plotted for comparison with linear theory. Typical error bars are indicated in the top-left corners of all three plots.

frequency of the waves approaches a constant value between $0.6N$ and $0.7N$. For larger Fr, the waves above topography were evanescent.

In the near lee of the hills, the frequency of the vertically propagating lee waves in subcritical flow approximately matched the frequency of the waves over the hills. For $\mathrm{Fr} > 1$, vertically propagating waves were still observed and were found to have approximately constant relative frequency $\omega/N \sim 0.57 \pm 0.05$.

Measuring the time difference between the leading trough and crest of the boundary-trapped lee wave, we estimated the frequency, ω_{lee}, of this undular disturbance. These values are compared the vertically propagating lee wave frequency, ω, in Fig. 6. Generally, we find the two match reasonably well in subcritical experiments implying that the frequency of the undular wave is set by the frequency of the waves over the hills. In supercritical experiments, however, the two frequencies do not match. Whereas ω/N remains nearly constant, ω_{lee}/N varies over a range of values between $0.6N$, and $0.9N$. In all experiments, however, there was no significant distinction between the effects of topographic shape.

The range of ω/N is consistent with experiments examining internal waves generated in the lee of a smooth step.[20] That study showed that waves were generated with frequencies approximately $0.6N$ for $\mathrm{Lo} > 1$ and $0.75N$ for $\mathrm{Lo} \lesssim 1$.

Figure 5(c) plots the relative frequency of waves in the far lee of the triangular and rectangular hills. Waves generated by turbulence in the lee of sinusoidal hills were less coherent in frequency. Like the waves in the immediate lee, we find that these smaller-scale waves are also generated within a narrow frequency range, independent of the topographic shape. In particular, the combined average relative frequency is $\omega/N \approx 0.72 \pm 0.05$. Such a narrow frequency range was also observed in the mixing box experiments of Dohan and Sutherland,[26] who found waves propagated away from a stationary turbulent mixed region with an average

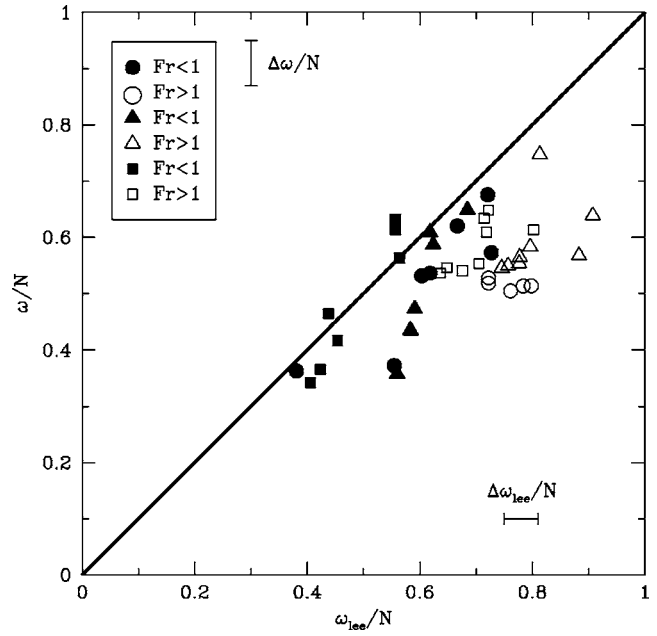

FIG. 6. Comparison of vertically propagating and boundary-trapped lee wave frequencies for subcritical and supercritical experiments using the large-amplitude sinusoidal, triangular, and rectangular hills as indicated by the shape of the plotted points.

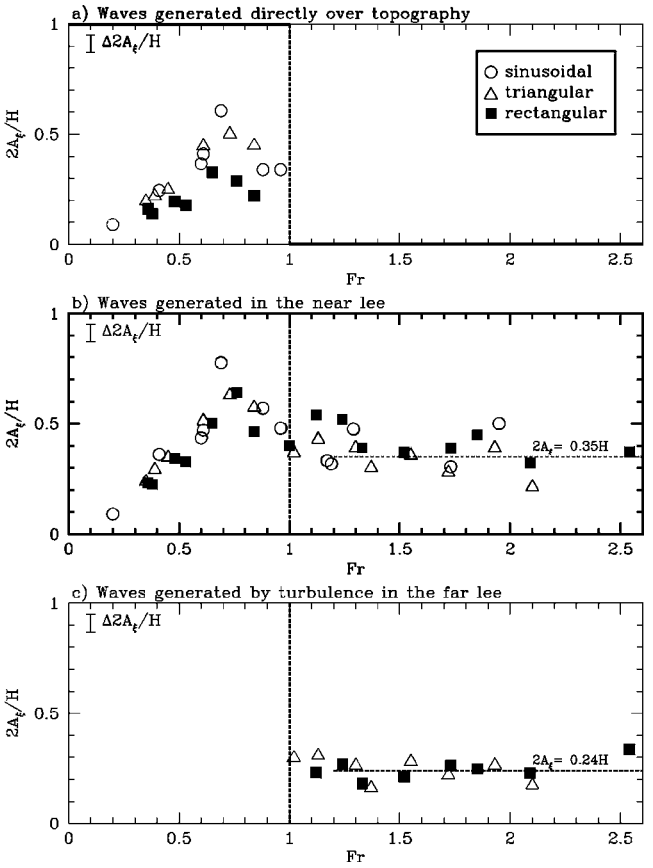

FIG. 7. Plots of the relative internal wave amplitude, $2A_\xi/H$, as a function of horizontal Froude number, Fr, for (a) waves generated directly over and (b) in the lee of large-amplitude topography with shapes indicated in the legend. The thick lines $2A_\xi/H=1$ and $2A_\xi/H=0$ are plotted in (a) to compare the experimental measurements with linear theory predictions for small-amplitude sinusoidal hills. The vertical dashed line in all three plots indicates the critical Froude number, Fr=1.

frequency of $\omega/N \approx 0.7$. This suggests that in supercritical flow a sufficiently rough surface creates vigorous turbulence which consequently becomes a source of internal waves.

As for the wave frequency analysis, the amplitudes of the waves were determined from data within time ranges taken over and in the near and far lee of the hills. Specifically, we computed the vertical displacement amplitude A_ξ of the vertically propagating waves and compared this with the half peak-to-peak hill height $H/2$. Figure 7 plots these relative wave amplitudes as a function of Fr. Linear theory predicts the relative amplitude over sinusoidal hills should be unity for $\mathrm{Fr}<1$ and zero for $\mathrm{Fr}>1$, as designated by the thick solid line in Fig. 7(a).

For $\mathrm{Fr}<1$, the waves generated over the hills have amplitudes significantly less than half the hill height. The discrepancy is particularly large in the rectangular hill experiments for which the maximum wave amplitude is $A_\xi \approx \frac{1}{3}(H/2)$. The amplitudes of waves generated by the sinusoidal and triangular hills are comparable but still much less than unity. In general, the amplitudes of the waves generated over the rectangular hills is two-thirds the corresponding amplitudes measured over the triangular and sinusoidal hills. The decreased wave amplitudes are the result of boundary layer separation that effectively changes the shape of the hill.

As shown in Fig. 7(b), for $\mathrm{Fr}<1$, the propagating lee wave amplitudes are consistently higher than those of the waves generated over the hills but in this case their amplitudes are approximately independent of topographic shape. This is because the structure of the boundary-trapped lee wave is similar in all three cases.

For $\mathrm{Fr}>1$, the topographic shape has a small but nonnegligible effect on the lee wave amplitudes. In particular, the average relative lee wave amplitudes for the sinusoidal, triangular, and rectangular hills are $2A_\xi/H \approx 0.39\pm0.11$, 0.33 ± 0.07, and 0.42 ± 0.07, respectively.

Figure 7(c) shows that there is no significant difference upon shape in the relative amplitude of waves generated by turbulence in the far lee, implying that topographic shape is important only insofar as providing a rough surface from which turbulence can be created. Generally we find the relative amplitude of the turbulence-generated waves is $2A_\xi/H \approx 0.24\pm0.06$.

These wave amplitudes are generally smaller than the lee wave amplitudes, when both are normalized by $H/2$. If instead we normalize the amplitude by the horizontal wavelength, we find that the resulting relative amplitudes of the lee and turbulence-generated waves are comparable, with $A_\xi \simeq 0.015\lambda_x$, as shown in Fig. 8.

Though, this may not seem large, the values are approximately 15% of the breaking amplitude as predicted by linear theory for overturning waves (designated by OT in Fig. 8) and for waves that become overturning due to interactions with the wave-induced mean flow.[32] This latter instability mechanism is called "self-acceleration" and is designated by SA in Fig. 8.

We also confirm the collapse of the data onto two narrow

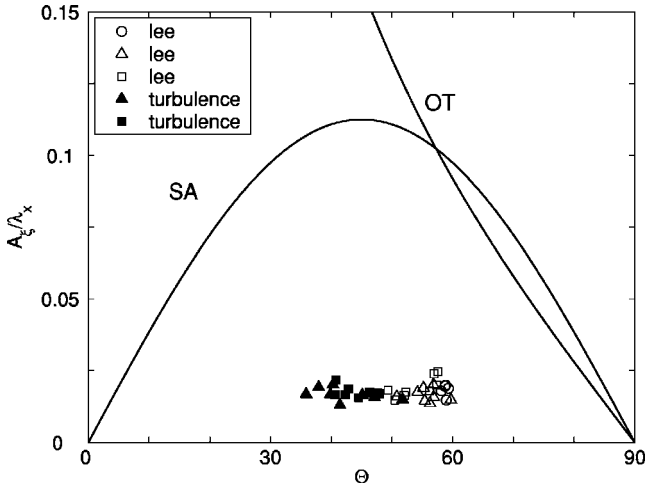

FIG. 8. Plot of relative wave amplitude, A_ξ/λ_x, as a function wave propagation angle, Θ, for dynamically generated waves. The curve denoted SA is the critical relative amplitude at which the waves should become unstable by self-acceleration. The curve denoted OT is the relative amplitude at which the waves should overturn.

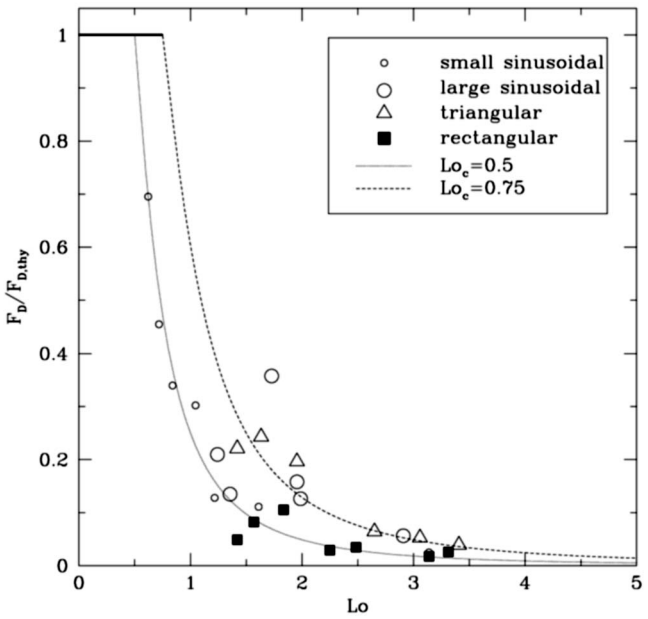

FIG. 9. Plot of nondimensional form drag, $F_D/F_{D,thy}$, versus Lo for all experiments with Fr<1. The thick solid line corresponds to linear theory, (7), the dotted line to (8) with $Lo_c=0.5$, and the dashed line to (8) with $Lo_c=0.75$.

ranges of propagation angles, $\Theta=55\pm3°$ ($\omega\approx0.57N$) for the waves generated in the near lee and $\Theta=43\pm3°$ ($\omega\approx0.72N$) for the waves generated in the far lee by the turbulent mixed region.

The amplitudes and narrow frequency ranges are consistent with other experimental measurements examining the dynamic generation of internal waves, as summarized in Table I.

C. Flow blocking

Throughout we have emphasized the importance of nonlinear effects, such as boundary layer separation, on wave generation. In the case where the boundary layer separates to form stagnant regions of fluid between successive hills, the effect decreases the resulting amplitude of the waves generated above, which consequently decreases the amount of momentum transported by the waves. The parameter that primarily controls boundary layer separation due to stratification is Lo.

Figure 9 plots the normalized drag, $F_D/F_{D,thy}$, as a function of Lo for all subcritical experiments (i.e., for Fr<1). Also plotted is the empirical prediction by Welch *et al.*[21] corresponding to $Lo_c=0.5$. For small-amplitude sinusoidal hills this curve fits the data quite well. For large amplitude hills, there is more scatter in the data. For sinusoidal and triangular hills, we find $Lo_c\simeq0.75$ more closely fits the data. As expected, Lo_c is smaller for rectangular hills because boundary layer separation is more pronounced behind such sharp corners. Typically we find that $Lo_c\simeq0.5$ is an adequate estimate of the critical Long's number for these experiments.

Comparable critical Long numbers have been measured in related studies of stratified flow over two-dimensional topography, including that of Bell and Thompson[34] for which $Lo_c=0.77$, Kimura and Mannins[35] for which $Lo_c=0.67$, and Welch *et al.*[21] for which $Lo_c\approx0.5-1.0$.

TABLE I. Angle of wave propagation and relative wave amplitude determined in five published experiments involving the dynamic generation of internal waves, and their comparison with the properties of internal waves in the near and far lee observed in this study.

Excitation mechanism	Θ (°)	A_ξ/λ_x
Stationary turbulence[a]	≈35	N/A
Stationary turbulence[b]	42–55	0.02–0.04
Turbulent shear flow[c]	46–60	0.003–0.03
Intrusive gravity current[d]	41–64	0.005–0.02
Lee of smooth step[e]	40–55	0.02–0.06
Lee of periodic hills	52–58	0.015–0.021
Turbulence	39–47	0.015–0.020

[a]Reference 24.
[b]Reference 26.
[c]Reference 25.
[d]Reference 33.
[e]Reference 20.

IV. CONCLUSIONS

Stratified flow over finite-amplitude periodic topography generates internal waves via three distinct mechanisms. The first mechanism is that of direct forcing over the hills which occurs only in subcritical experiments with Fr<1. In this case linear theory well predicts the wave frequency for Fr $\lesssim0.7$ and the relative frequency $\omega/N\simeq0.7$ for $0.7\lesssim$Fr<1. The amplitude is poorly predicted however because the corresponding Long number is large and so boundary-layer separation enhanced by stratification occurs. The discrepancy in amplitude[22] and resulting wave-induced drag is large even for sinusoidal hills with $H/L=0.1$. When boundary separa-

tion occurs the separated streamline thus acts as a lower boundary rather than the surface of the hills themselves, and so the hill height is effectively reduced.

In either subcritical or supercritical flow, we observed the generation of vertically propagating waves in the near lee of the hills. Their frequencies were set by the excitation frequency for $\mathrm{Fr}<0.7$ and held approximately constant values about $0.55N$ for $\mathrm{Fr}>0.7$. The relative amplitude of these waves was generally largest in the lee of the rectangular hills. Over all experiments we found $A_\xi \simeq 0.35H/2$.

When $\mathrm{Fr}>1$, the flow in the far lee of the hills was sufficiently turbulent to excite moderately large amplitude waves. Their relative frequency lay within narrow range slightly larger than that for waves in the near lee. Generally, we find $\omega/N \approx 0.72 \pm 0.05$ and the corresponding angle of propagation is $\Theta \approx 43 \pm 3°$.

The comparison of our results with other studies reveals a universal trend in the characteristic frequency of waves generated by dynamic mechanisms. This suggests that internal waves are generated by turbulence through a resonant feedback mechanism that most strongly excites waves in a narrow frequency band. In particular, because waves having $\Theta = 45°$ transport the greatest amount of horizontal momentum away from their source they may act most efficiently in modifying the turbulence in a way that enhances their excitation.[27]

The close agreement between experiments with triangular and sinusoidal hills, gives some encouragement that a heuristic modification of linear theory could be used to account for blocking between mountain ranges. On the other hand, the discrepancy observed with rectangular hill experiments implies that further modification would be required to empirically capture the dynamics of wave generation above chasms such as those in the mid-Atlantic ridge. Nonetheless, the results plotted in Fig. 8 show that such waves share universal characteristics regarding their frequency relative to N and their amplitude relative to their horizontal wavelength.

ACKNOWLEDGMENTS

This work has been supported by the Natural Sciences and Engineering Research Council of Canada (NSERC), the Canadian Foundation for Climate and Atmospheric Science (CFCAS), and the Alberta Ingenuity Studentship program.

[1] N. A. McFarlane, "The effect of orographically excited gravity wave drag on the general circulation of the lower stratosphere and troposphere," J. Atmos. Sci. **44**, 1775 (1987).
[2] C. McLandress, "On the importance of gravity waves in the middle atmosphere and their parameterization in general circulation models," J. Atmos. Sol.-Terr. Phys. **60**, 1357 (1998).
[3] S. G. Llewellyn Smith and W. R. Young, "Conversion of the barotropic tide," J. Phys. Oceanogr. **32**, 1554 (2002).
[4] N. J. Balmforth, G. R. Ierley, and W. R. Young, "Tidal conversion by subcritical topography," J. Phys. Oceanogr. **32**, 2900 (2002).
[5] L. St. Laurent and C. Garrett, "The role of internal tides in mixing the deep ocean," J. Phys. Oceanogr. **32**, 2882 (2002).
[6] L. St. Laurent, S. Stringer, C. Garrett, and D. Perrault-Joncas, "The generation of internal tides at abrupt topography," Deep-Sea Res., Part I **50**, 987 (2003).
[7] S. Legg and A. Adcroft, "Internal wave breaking at concave and convex continental slopes," J. Phys. Oceanogr. **33**, 2224 (2003).
[8] S. Legg, "Internal tides generated on a corrugated slope. Part I: Cross-slope barotropic forcing," J. Phys. Oceanogr. **34**, 156 (2004).
[9] A. L. New and J. C. B. DaSilva, "Remote-sensing evidence for the local generation of internal soliton packets in the central Bay of Biscay," Deep-Sea Res., Part I **49**, 915 (2002).
[10] D. L. Rudnick, T. J. Boyd, R. E. Brainard, G. S. Carter, G. D. Egbert, M. C. Gregg, P. E. Holloway, J. M. Klymak, E. Kunze, C. M. Lee, M. D. Levine, D. S. Luther, J. P. Martin, M. A. Merrifield, J. N. Moum, J. D. Nash, R. Pinkel, L. Rainville, and T. B. Sanford, "From tides to mixing along the Hawaiian ridge," Science **301**, 355 (2003).
[11] J. R. Ledwell, E. Montgomery, K. Polzin, L. C. St. Laurent, R. Schmitt, and J. Toole, "Evidence for enhanced mixing over rough topography in the abyssal ocean," Nature (London) **403**, 179 (2000).
[12] J. M. Klymak and M. C. Gregg, "Tidally generated turbulence over the Knight Inlet sill," J. Phys. Oceanogr. **34**, 1135 (2004).
[13] A. C. N. Garabato, K. L. Polzin, B. A. King, K. J. Heywood, and M. Visbeck, "Widespread intense turbulent mixing in the Southern Ocean," Science **303**, 210 (2004).
[14] A. E. Gill, *Atmosphere-Ocean Dynamics* (Academic, San Diego, 1982).
[15] R. R. Long, "Some aspects of the flow of stratified fluids. a theoretical investigation," Tellus **5**, 42 (1953).
[16] P. G. Baines, *Topographic Effects in Stratified Flows* (Cambridge University Press Cambridge, England, 1995).
[17] R. R. Long, "Some aspects of the flow of stratified fluids. III Continuous density gradients," Tellus **7**, 341 (1955).
[18] R. R. Long, "Blocking effects in flow over obstacles," Tellus **22**, 471 (1970).
[19] P. G. Baines and K. P. Hoinka, "Stratified flow over two-dimensional topography in fluid of infinite depth: A laboratory simulation," J. Atmos. Sci. **42**, 1614 (1985).
[20] B. R. Sutherland, "Large-amplitude internal wave generation in the lee of step-shaped topography," Geophys. Res. Lett. **29**, 1769 (2002).
[21] W. T. Welch, P. Smolarkiewicz, R. Rotunno, and B. A. Boville, "The deepening of a mixed layer in a stratified fluid," J. Atmos. Sci. **58**, 1477 (2001).
[22] D. Aguilar, B. R. Sutherland, and D. J. Muraki, "Generation of internal waves over sinusoidal topography," Deep-Sea Res., Part II **53**, 96 (2006).
[23] D. J. Carruthers and J. C. R. Hunt, "Velocity fluctuations near an interface between a turbulent region and a stably stratified layer," J. Fluid Mech. **165**, 475 (1986).
[24] P. F. Linden, "The deepening of a mixed layer in a stratified fluid," J. Fluid Mech. **71**, 385 (1975).
[25] B. R. Sutherland and P. F. Linden, "Internal wave generation by flow over a thin barrier," J. Fluid Mech. **377**, 223 (1998).
[26] K. Dohan and B. R. Sutherland, "Internal waves generated from a turbulent mixed region," Phys. Fluids **15**, 488 (2003).
[27] K. Dohan, "Internal wave generation from a turbulent mixed region," Ph.D. thesis, University of Alberta (2004).
[28] G. Oster, "Density gradients," Sci. Am. **213**, 70 (1965).
[29] S. B. Dalziel, "Rayleigh-Taylor instability: Experiments with image analysis," Dyn. Atmos. Oceans **20**, 127 (1993).
[30] S. B. Dalziel, G. O. Hughes, and B. R. Sutherland, "Whole field density measurements," Exp. Fluids **28**, 322 (2000).
[31] B. R. Sutherland, S. B. Dalziel, G. O. Hughes, and P. F. Linden, "Visualization and measurement of internal waves by "synthetic Schlieren." Part 1: Vertically oscillating cylinder," J. Fluid Mech. **390**, 93 (1999).
[32] B. R. Sutherland, "Finite-amplitude internal wavepacket dispersion and breaking," J. Fluid Mech. **429**, 343 (2001).
[33] M. R. Flynn and B. R. Sutherland, "Intrusive gravity currents and internal wave generation in stratified fluid," J. Fluid Mech. **514**, 355 (2004).
[34] R. C. Bell and R. O. Thompson, "Valley ventilation by cross winds," J. Fluid Mech. **96**, 757 (1980).
[35] F. Kimura and P. Mannins, "Blocking in periodic valleys," Boundary-Layer Meteorol. **44**, 137 (1980).